

Theoretical simulation on the variation in the transport behavior under pressure and magnetic field in $\text{La}_{0.825}\text{Sr}_{0.175}\text{MnO}_3$

Jing-Yi Wang, Chun-Lian Hu, Kui-Juan Jin,^{a)} Hui-Bin Lu, Cong Wang, Rui-Qiang Zhao, and Guo-Zhen Yang

Beijing National Laboratory for Condensed Matter Physics, Institute of Physics, Chinese Academy of Science, P.O. Box 603, Beijing 100190, China

(Received 13 March 2010; accepted 26 April 2010; published online 3 June 2010)

Based on phase separation model and breadth-first traversal algorithm, the spin-related electron transport property of $\text{La}_{0.825}\text{Sr}_{0.175}\text{MnO}_3$ under hydrostatical pressure and magnetic field was systematically simulated. We find that the external hydrostatical pressure has a more important influence on the residual resistivity, high temperature resistivity coefficient, activation energy, and electron scattering of $\text{La}_{0.825}\text{Sr}_{0.175}\text{MnO}_3$ than the external magnetic field. However, the Curie temperature and the magnon scattering are more sensitive to the external magnetic field than to the external hydrostatical pressure in $\text{La}_{0.825}\text{Sr}_{0.175}\text{MnO}_3$. © 2010 American Institute of Physics. [doi:10.1063/1.3432751]

The perovskite manganites usually have a metal-insulator transition accompanied by a simultaneous phase to phase transition under various temperature, magnetic field,¹⁻³ optical field,^{4,5} and external pressure.⁶⁻¹⁰ Moreover, they exhibit novel characteristics such as colossal magnetoresistance (CMR) and photon induced phase transition.^{4,5} The intrinsic mechanism of the CMR, which has been observed by many groups,¹¹⁻¹⁵ is widely known as the phase separation.

The pressure-induced phase separation has been paid much attention due to its potential application in device designing. It has been investigated that the resistivity of $\text{La}_{0.825}\text{Sr}_{0.175}\text{MnO}_3$ decreases with the increase in the hydrostatic pressure and magnetic field, respectively.⁶ However, a systematic theoretical study is still absent. In our previous work,¹⁶⁻¹⁸ by introducing the phase separation model and a breadth-first traversal (BFT) algorithm, the electric transport in many perovskite oxide systems such as $\text{La}_{1-x}\text{Ca}_x\text{MnO}_3$ (LCMO) and $\text{La}_{1-x}\text{Te}_x\text{MnO}_3$ (LTMO) under the magnetic field has been theoretical studied.

In this paper, based on phase separation model, the resistivity dependence on the hydrostatical pressure and the magnetic field for $\text{La}_{0.825}\text{Sr}_{0.175}\text{MnO}_3$ is simulated, and the results agree well with the experimental data. It is found that the pressure has a more important influence on the electron scattering coefficient, the high temperature resistivity coefficient, and the activation energy than the magnetic field. And the Curie temperature and the magnon scattering coefficient are more sensitive to the magnetic field than to the external hydrostatical pressure.

The actual system is simulated as a $N \times N$ (in our simulation, $N=500$) matrix grid. At very low temperature, the system is almost with a single phase, the ferromagnetic (FM) phase. At very high temperature, most part of the system is occupied by the other phase, the paramagnetic (PM) phase. In the middle temperature region, the two phases coexist.

With the increase in temperature, more and more grids are changed from FM phase to the PM one. A parameter P , which is defined as the number of FM grids over the number of total grids, represents the fraction of the FM metallic sites ($0 \leq P \leq 1$). The parameter P dependence on temperature is written as

$$P(T) = \frac{1}{1 + B \exp[A(T - T_c)]},$$

where T_c is the Curie temperature. The parameter A is the result of a fitting procedure,¹⁶ and the parameter B is related to the critical value $P(T_c)$ for percolation, which is defined as $B = [1 - P(T_c)] / P(T_c)$.

The resistivity in FM phase is written as $\rho_M(T) = \rho_{m0} + \rho_{m1}T^2 + \rho_{m2}T^{4.5}$,^{1,16-18} where ρ_{m0} is the residual resistivity independent of the temperature, which originates from the electron scattering among the domains and the impurity's scattering, ρ_{m1} denotes the electron-electron scattering coefficient¹⁹ and ρ_{m2} represents the magnon scattering coefficient involving the phonon scattering,²⁰ respectively. The $T^{3.5}$ is also described as the magnon scattering in some systems,²¹ especially in the FM metallic state.²² However, in some perovskite oxides, by using T^2 and $T^{4.5}$,^{1,23} the resistivity dependence on temperature has been described successfully. In our previous work,¹⁶⁻¹⁸ by simply taking the electron-electron scattering ($\rho_{m1}T^2$) and the magnon scattering ($\rho_{m2}T^{4.5}$) in LCMO and LTMO, the experiment data have also been successfully simulated. Thus, in low-temperature FM phase of the present material $\text{La}_{0.825}\text{Sr}_{0.175}\text{MnO}_3$, for simplicity, the electrical transport mechanism is described only by $\rho_{m1}T^2$ and $\rho_{m2}T^{4.5}$. The small polaron model is employed to simulate the electronic transport in PM phase. The resistivity in the PM phase is $\rho_I(T) = \rho_{i0}T \exp(E_0/k_B T)$, where ρ_{i0} is the high temperature resistivity coefficient, E_0 is the activation energy, and k_B represents the Boltzmann constant.^{24,25} It has been well understood that the scattering coefficients is determined by the energy band near the Fermi face, and the energy band is mainly determined by

^{a)}Author to whom correspondence should be addressed. Electronic mail: kjjin@aphy.iphy.ac.cn.

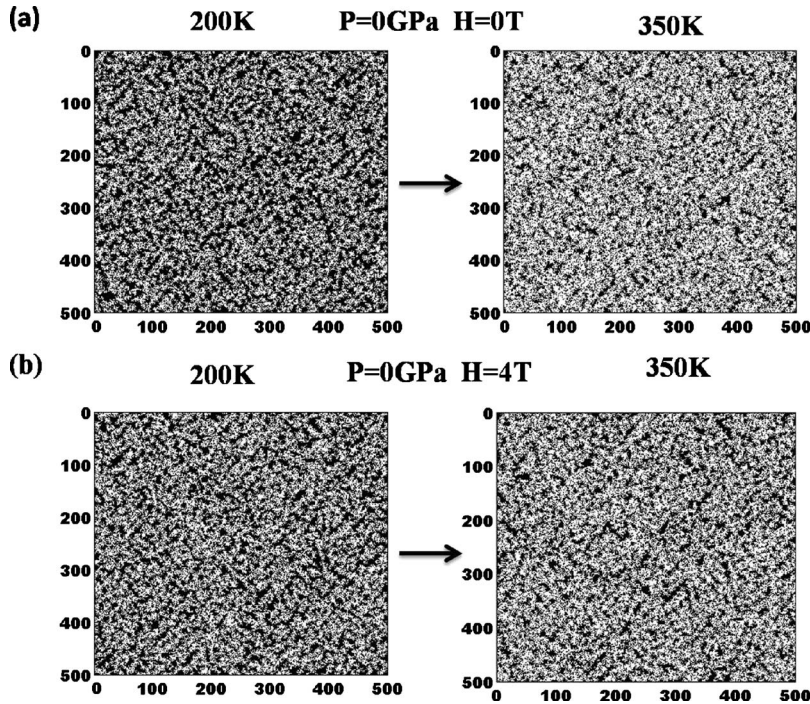


FIG. 1. Simulated process of percolation from low temperature FM (black) to high temperature PM (white) phase transition in the mixed phase description in a 500×500 matrix under (a) zero magnetic field and (b) 4 T magnetic field with zero pressure, respectively. The arrows indicate the warming process from 200 to 350 K.

bondlength, bond angle, hopping integral, etc.^{19,20,26} The Mn–O bond length decreases with the increase in pressure.^{27,28} With the increase in the applied magnetic field, the bond angle decreases and the value of the hopping integral increases, respectively.²⁹

In our calculation, the residual resistivity can be derived from the experimental data. Under the zero pressure and magnetic field, the other parameters used in our simulation are obtained from the Refs. 6 and 25. The total effective resistivity is determined by the parallel connection of the two parts of FM and PM phase. Using the BFT algorithm,^{16–18} the total resistivity is obtained.

Figure 1 shows the simulated percolation process of $\text{La}_{0.825}\text{Sr}_{0.175}\text{MnO}_3$ with (a) zero magnetic field and (b) 4 T magnetic field with zero pressure, respectively. It can be seen

from Fig. 1 that the system undergoes a transition from a FM state at low temperature of 200 K to a PM state at high temperature of 350 K for both the system with zero and 4 T magnetic field with zero pressure.

Figures 2(a) and 2(b) show the experimental⁶ and theoretical resistivity (ρ) versus temperature (T) in the $\text{La}_{0.825}\text{Sr}_{0.175}\text{MnO}_3$ at different external hydrostatical pressure and magnetic field, respectively. The parameters under different external hydrostatical pressure and magnetic field are given in the Table I. From Fig. 2 it can be seen that the theoretical results are in good agreement with the experiment data.

The Curie temperature (T_c) versus the pressure and the magnetic field for $\text{La}_{0.825}\text{Sr}_{0.175}\text{MnO}_3$ are shown in Fig. 3.

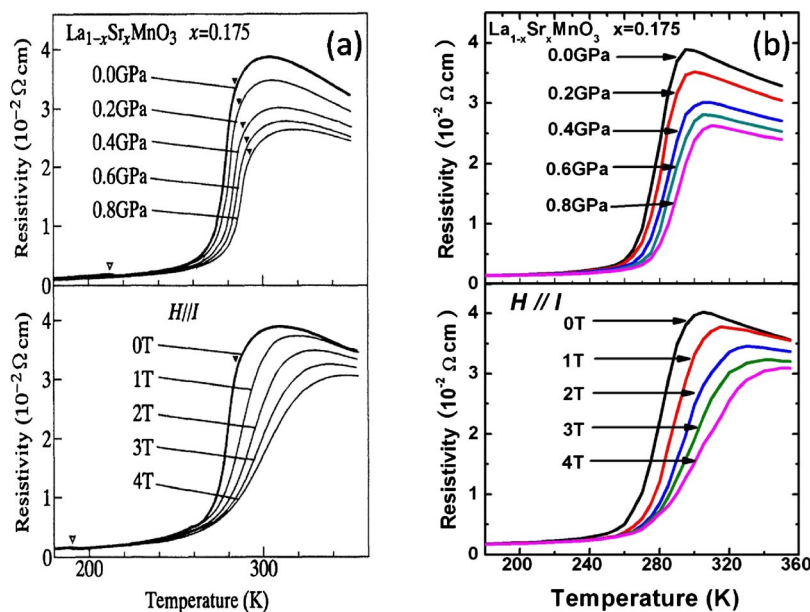


FIG. 2. (Color online) The experimental (a) (obtained from Ref. 6) and simulated (b) resistivity dependence on temperature for $\text{La}_{0.825}\text{Sr}_{0.175}\text{MnO}_3$ at various external hydrostatical pressure and the magnetic field.

TABLE I. (a) Parameters used in the simulation under different external hydrostatical pressure. (b) Parameters used in the simulation under different external magnetic field.

T_c (K)	H (T)	P_0	ρ_{m0} ($10^{-2} \Omega \text{ cm}$)	ρ_{m1} ($10^{-2} \Omega \text{ cm K}^{-2}$)	ρ_{m2} ($10^{-2} \Omega \text{ cm K}^{-4.5}$)	E_0 (meV)	ρ_{i0} ($10^{-2} \Omega \text{ cm}$)
(a)							
278	0	0.455	0.150	5.65×10^{-10}	4.32×10^{-13}	25.16	2.90×10^{-3}
281	0.2	0.455	0.148	4.45×10^{-10}	3.62×10^{-13}	22.84	2.83×10^{-3}
284	0.4	0.455	0.147	1.65×10^{-10}	2.32×10^{-13}	19.65	2.72×10^{-3}
286	0.6	0.455	0.146	9.05×10^{-11}	1.62×10^{-13}	17.75	2.68×10^{-3}
289	0.8	0.455	0.145	8.20×10^{-11}	1.52×10^{-13}	16.29	2.64×10^{-3}
(b)							
280	0	0.455	0.161	5.85×10^{-10}	4.32×10^{-13}	24.13	2.90×10^{-3}
287	1	0.455	0.1595	5.15×10^{-10}	5.62×10^{-14}	23.27	2.89×10^{-3}
293	2	0.455	0.1575	4.75×10^{-10}	4.62×10^{-14}	21.97	2.87×10^{-3}
297	3	0.455	0.1570	3.85×10^{-10}	2.62×10^{-14}	21.37	2.85×10^{-3}
302	4	0.455	0.1560	3.25×10^{-10}	1.62×10^{-14}	20.51	2.82×10^{-3}

Owing to the increase in the external hydrostatical pressure, the Mn–O bond is shortened, so the exchange integration between the Mn^{3+} and the Mn^{4+} increases. According to the band theory, we can conclude the e_g band width increases. Therefore, the Curie temperature (T_c) increases. Moreover, from our simulation, it is found that the Curie temperature is more sensitive to the magnetic field than to the pressure.

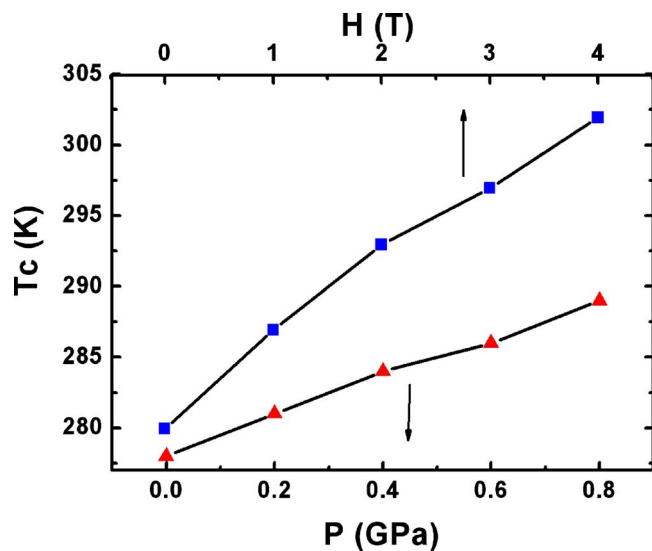
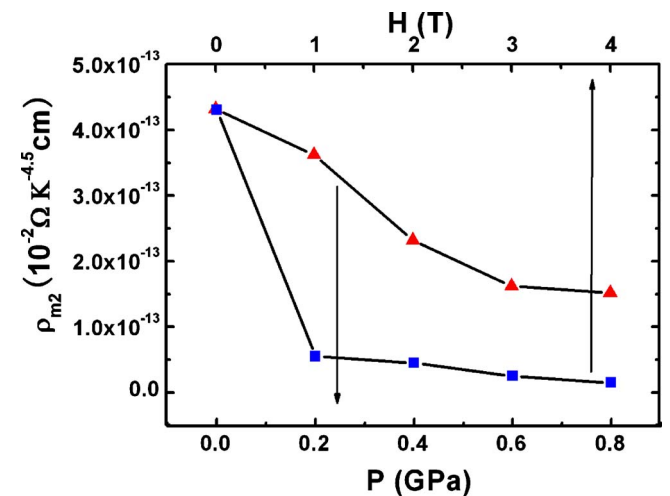
The magnon scattering coefficient (ρ_{m2}) dependence on the pressure and the magnetic field for $\text{La}_{0.825}\text{Sr}_{0.175}\text{MnO}_3$ are shown in Fig. 4. It can be seen that the magnon scattering coefficient decreases more rapidly with the increase in the magnetic field than that with the pressure. With the increase in the pressure and the magnetic field, the magnon scattering decreases due to the ordered core spins.²⁰

Figure 5 shows the dependence of the electron scattering coefficient (ρ_{m1}) on the pressure and the magnetic field in the $\text{La}_{0.825}\text{Sr}_{0.175}\text{MnO}_3$. It can be seen that the electron scattering coefficient decreases with the increase in the pressure and the magnetic field. Moreover, the pressure has a stronger influ-

ence on the electron scattering coefficient than the magnetic field.

The variation in residual resistivity (ρ_{m0}) versus the pressure and the magnetic field for the $\text{La}_{0.825}\text{Sr}_{0.175}\text{MnO}_3$ is plotted in Fig. 6. It decreases with the increase in the pressure and the magnetic field, and the decreasing rates for each of them are comparable. With the increase in the magnetic field, the spin scattering between different domains gets decreased, as well as the resistivity of the FM phase. The external hydrostatical pressure can shorten the Mn ion spacing, so the bandwidth of e_g is increased, and electrons and holes are delocalized, resulting in a decrease in the resistivity.

Figure 7 shows the high temperature resistivity coefficient (ρ_{i0}) dependence on the pressure and the magnetic field in the $\text{La}_{0.825}\text{Sr}_{0.175}\text{MnO}_3$. It can be seen that the high temperature resistivity coefficient decreases with the increase in the pressure and the magnetic field. Moreover, the decreasing rate is larger with the increase in the pressure than that with the magnetic field. This can be explained as follows. With the increase in the pressure, the lattice constant is decreased and the interaction between atoms is increased. From a

FIG. 3. (Color online) The Curie temperature T_c dependence on the external hydrostatical pressure and the magnetic field for $\text{La}_{0.825}\text{Sr}_{0.175}\text{MnO}_3$.FIG. 4. (Color online) The magnon scattering coefficient dependence on the external hydrostatical pressure and the magnetic field in $\text{La}_{0.825}\text{Sr}_{0.175}\text{MnO}_3$.

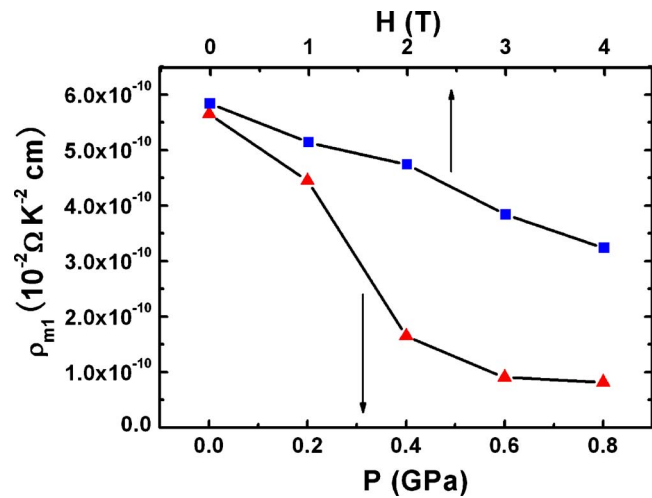


FIG. 5. (Color online) The variation in the electron scattering coefficient with the external hydrostatical pressure and the magnetic field for $La_{0.825}Sr_{0.175}MnO_3$.

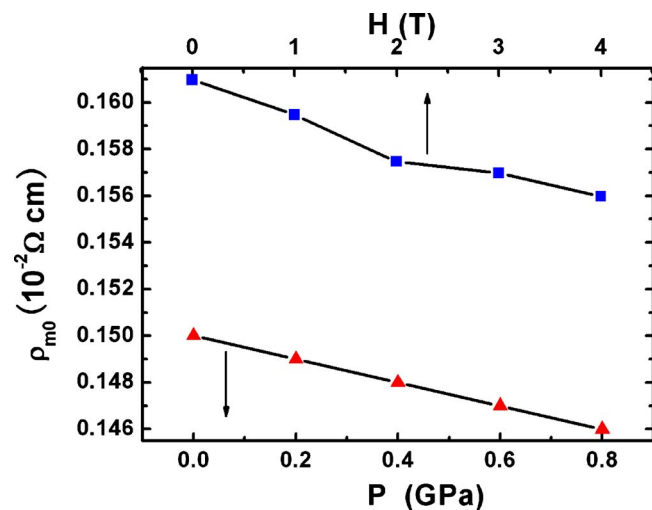


FIG. 6. (Color online) The residual resistivity dependence on external hydrostatical pressure and the magnetic field for $La_{0.825}Sr_{0.175}MnO_3$.

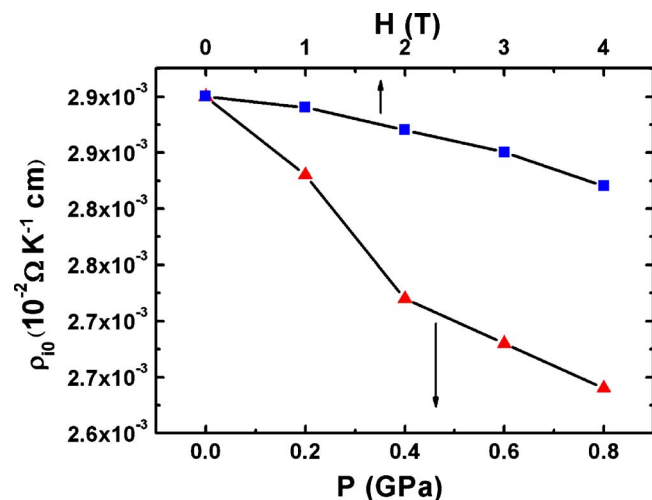


FIG. 7. (Color online) The variation in the high temperature resistivity coefficient with the external hydrostatical pressure and the magnetic field for $La_{0.825}Sr_{0.175}MnO_3$.

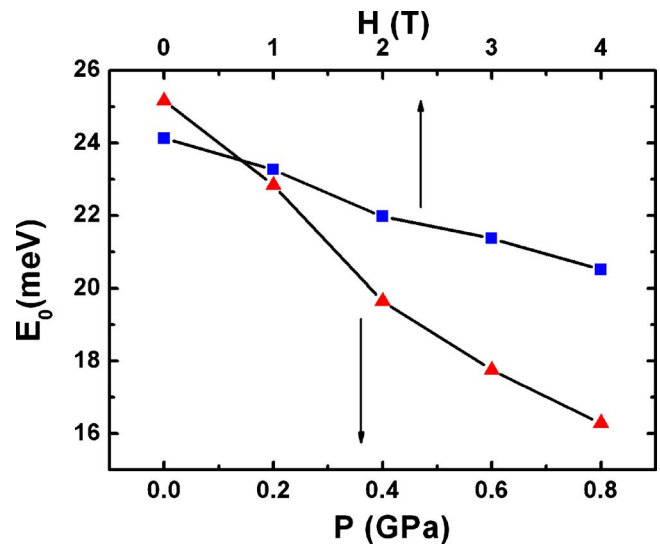


FIG. 8. (Color online) The dependence of the activation energy E_0 with external hydrostatical pressure and the magnetic field in $La_{0.825}Sr_{0.175}MnO_3$.

simple view of tight bonding theory, the width of the energy band gets increased, the band gap of the PM phase as a semiconductor gets decreased, as well as the resistivity of the $La_{0.825}Sr_{0.175}MnO_3$.

Activation energy (E_0) versus the pressure and the magnetic field in the $La_{0.825}Sr_{0.175}MnO_3$ is shown in Fig. 8. It decreases with the increase in the pressure and the magnetic field. The dependence of the activation energy on the pressure can be easily understood in the following way. With the increase in the pressure, the nearest atoms get more closed, and the transfer integral is larger so that the activation energy is decreased.²⁹ The reason for the dependence of the activation energy on the magnetic field in $La_{0.825}Sr_{0.175}MnO_3$ has not been well understood yet, and the further study to reveal the physics origin about it should be expected.

In summary, based on the phase separation scenario, the temperature dependence of the resistivity of $La_{0.825}Sr_{0.175}MnO_3$ under various values of the external hydrostatical pressure and those of the magnetic field is simulated and the theoretical results are in good agreement with the experimental results. It is found that the electron scattering coefficient, the high temperature resistivity coefficient, and the activation energy decrease more rapidly with the increase in external hydrostatical pressure than that of the magnetic field. However, the Curie temperature and the magnon scattering coefficient are more sensitive to the magnetic field than to the external hydrostatical pressure. Moreover, small polaron mechanism plays a dominant role in the transport property of PM insulating phase in the high temperature region.

ACKNOWLEDGMENTS

This work has been supported by the National Natural Science Foundation of China (Grant No. 10825418) and National Basic Research Program of China.

¹P. Schiffer, A. P. Ramirez, W. Bao, and S.-W. Cheong, *Phys. Rev. Lett.* **75**, 3336 (1995).

²Z. Q. Mao, M. Zhou, J. Hooper, V. Golub, and C. J. O'Connor, *Phys. Rev.*

- Lett.* **96**, 077205 (2006).
- ³S. Mukhopadhyay and I. Das, *Europhys. Lett.* **83**, 27003 (2008).
- ⁴V. Kiryukhin, D. Casa, J. P. Hill, B. Vigiante, Y. Tomioka, and Y. Tokura, *Nature (London)* **386**, 813 (1997).
- ⁵K. Miyano, T. Tanaka, Y. Tomioka, and Y. Tokura, *Phys. Rev. Lett.* **78**, 4257 (1997).
- ⁶Y. Moritomo and A. Asamitsu, *Phys. Rev. B* **51**, 16491 (1995).
- ⁷V. Markovich, E. Rozenberg, A. I. Shames, and G. Gorodetsky, *Phys. Rev. B* **65**, 144402 (2002).
- ⁸F. J. Rueckert, M. Steiger, B. K. Davis, T. Huynh, J. J. Neumeier, and M. S. Torikachvili, *Phys. Rev. B* **77**, 064403 (2008).
- ⁹M. Filippi, W. Prellier, P. Auban-Senzier, and C. R. Pasquier, *Appl. Phys. Lett.* **93**, 142110 (2008).
- ¹⁰L. Malavasi, M. Baldini, I. Zardo, M. Hanfland, and P. Postorino, *Appl. Phys. Lett.* **94**, 061907 (2009).
- ¹¹A. Urushibara, Y. Moritomo, T. Arima, A. Asamitsu, G. Kido, and Y. Tokura, *Phys. Rev. B* **51**, 14103 (1995); V. Y. Ivanov, V. D. Travkin, A. A. Mukhin, S. P. Lebedev, A. A. Volkov, A. Pimenov, A. Loidl, A. M. Balbashov, and A. V. Mozhaev, *J. Appl. Phys.* **83**, 7180 (1998); E. S. Itskevich, V. F. Kraidenov, and S. M. Kuzmin, *Low Temp. Phys.* **32**, 928 (2006).
- ¹²M. Fäth, S. Freisem, A. A. Menovsky, Y. Tomioka, J. Aarts, and J. A. Mydosh, *Science* **285**, 1540 (1999).
- ¹³L. Zhang, C. Isrel, A. Biswas, R. L. Greene, and A. D. Lozanne, *Science* **298**, 805 (2002).
- ¹⁴C. Renner, G. Aeppli, B.-G. Kim, Y.-A. Soh, and S.-W. Cheong, *Nature (London)* **416**, 518 (2002).
- ¹⁵M. Mayr, A. Moreo, J. A. Verges, J. Arispe, A. Feiguin, and E. Dagotto, *Phys. Rev. Lett.* **86**, 135 (2001).
- ¹⁶Q. L. Zhou, K. J. Jin, K. Zhao, D. Y. Guan, H. B. Lu, Z. H. Chen, and G. Z. Yang, *Phys. Rev. B* **72**, 224439 (2005).
- ¹⁷Q. L. Zhou, K. Zhao, K. J. Jin, D. Y. Guan, H. B. Lu, Z. H. Chen, and G. Z. Yang, *Appl. Phys. Lett.* **87**, 172510 (2005).
- ¹⁸Q. L. Zhou, D. Y. Guan, K. J. Jin, K. Zhao, Z. H. Chen, H. B. Lu, Y. L. Zhou, P. Han, and G. Z. Yang, *Chin. Phys. Lett.* **22**, 1749 (2005).
- ¹⁹A. H. Thompson, *Phys. Rev. Lett.* **35**, 1786 (1975).
- ²⁰K. Kubo and N. Ohata, *J. Phys. Soc. Jpn.* **33**, 21 (1972).
- ²¹X. J. Chen, H.-U. Habermeier, C. L. Zhang, H. Zhang, and C. C. Almasan, *Phys. Rev. B* **67**, 134405 (2003).
- ²²F. J. Dyson, *Phys. Rev.* **102**, 1217 (1956).
- ²³G. Jeffrey Synder, R. Hiskes, S. DiCarolis, M. R. Beasley, and T. H. Geballe, *Phys. Rev. B* **53**(21), 14434 (1996).
- ²⁴G. Jakob, W. Westerberg, F. Martin, and H. Adrian, *Phys. Rev. B* **58**, 14966 (1998).
- ²⁵P. Mandal, B. Bandyopadhyay, and B. Ghosh, *Phys. Rev. B* **64**, 180405(R) (2001).
- ²⁶W. E. Lawrence and J. W. Wilkins, *Phys. Rev. B* **7**, 2317 (1973).
- ²⁷C. W. Cui, T. A. Tyson, Z. Zhong, J. P. Carlo, and Y. H. Qin, *Phys. Rev. B* **67**, 104107 (2003).
- ²⁸J. M. De Teresa, M. R. Ibarra, J. Blasco, J. García, C. Marquina, and P. A. Algarabel, *Phys. Rev. B* **54**, 1187 (1996).
- ²⁹Y. H. Sun, Y. G. Zhao, H. F. Tian, C. M. Xiong, B. T. Xie, M. H. Zhu, S. Park, W. D. Wu, J. Q. Li, and Q. Li, *Phys. Rev. B* **78**, 024412 (2008).